(Received 11 August 2024, Accepted 4 September 2024, Scheduled 13 September 2024)

Two-Port Hexagon-Shaped MIMO Antenna for UWB Applications Integrated with Four Frequently-Used Stopbands for Medical Domains

Liangliang Zhao[1,*], Aidong Li[1], Yongmao Wang[1], Dengyang Song[1], Mingxuan Zheng[2], Chenlu Liu[1], Chuwei Li[3], Yongtao Liang[1], Huiling Zhao[1], and Chufeng Hu[4]

[1]*School of Electronics and Information, Northwestern Polytechnic University, Xi'an, China*
[2]*System Engineering Division, Xi'an Electronic Engineering Research Institute, Xi'an, China*
[3]*China Academy of Space Technology (CAST), Beijing, China*
[4]*Science and Technology on UAV Laboratory, Northwestern Polytechnic University, Xi'an, China*

ABSTRACT: A compact ultra-wideband (UWB) multiple-input multiple-output (MIMO) antenna with four stopbands is designed and experimentally investigated. By the method of coating, various T-shaped structures and split-ring resonators (SRRs) are used for suppressing the mutual coupling and introducing the band-notched characteristics, respectively. The actual design has an overall size of $46 \times 37 \times 1.57\,\text{mm}^3$ across the whole UWB spectrum from 2 to 22 GHz except stopbands from 3.47 to 3.83 GHz, 5.2 to 5.85 GHz, 7.19 to 7.84 GHz, and 8.15 to 8.6 GHz, which prevent the interference of Microwave Access (WiMax), wireless local area network (WLAN), satellite downlink, and satellite communications band (ITU 8 GHz) bands, respectively. Besides, the isolation of the most operating frequencies is higher than 20 dB, and the antenna obtains a fairly stable radiation pattern and gain, as well as a lower envelope correlation coefficient (ECC < 0.005). Additionally, using the antenna inserted in name badge of the doctor, the chance of infection will be greatly reduced. Ultimately, the proposed MIMO monopole antenna has a potential application in the medical domain.

1. INTRODUCTION

In recent years, UWB antenna has received increasing attention as the result of its higher data transmission capacities, wide operational bandwidth, and low cost. However, UWB antenna still faces the shortcomings of poor reliability and multipath fading [1–3]. To circumvent these issues, an effective method called MIMO technology is presented. Therefore, it is of great meaning to combine UWB and MIMO technology. With the decrease of MIMO antenna size, mutual coupling effect can deteriorate the performance of MIMO antenna. Various decoupling methods have been employed like a vertical slot etched on the ground [4, 5], broadband neutralization line [6], without any decoupling structure [7–10], inverted T-shaped slot [11], T-shaped strip introduced between radiating elements [12–16], rectangle stub employed between CPW-fed radiating elements [17], etc. Besides, polarization diversity technology can be utilized to attain high isolation by placing the antenna vertically [18]. Meanwhile, owing to the case that the UWB-MIMO system is lightly sensitive to undesired signals such as Microwave Access (WiMAX), wireless local area network (WLAN), and X-bands for satellite communication, the stop filter technology is created to suppress the interference, attracting a great deal of attention and interests [19]. There are plenty of methods to create stopbands for UWB antennas. One is to cut slots on the feed line, radiating patch, and ground [20–23], which will also induce current to concentrate near slots and reject undesired signals. Another is to add parasitic elements [24–26], concentrating current on the additional parasitic elements at a prescribed frequency point, constraining the electromagnetic wave here and blocking it from radiating, introducing a stopband. As the antennas become more miniaturized, the generation of more stop bands is limited.

Consequently, a tapered fed two-port UWB MIMO antenna is proposed and assembled for UWB applications with four stopband superiorities. Particularly, by loading T-shaped structures and T-shaped slots, the antenna has an ultra-wide operating band from 2 to 22 GHz with a compact dimension of $46 \times 37 \times 1.57\,\text{mm}^3$. Furthermore, by the method of etching various slots and adding split-ring resonators (SRRs), the antenna provides the exact stopbands for preventing the interference of WiMax, WLAN, satellite downlink, and ITU 8 GHz (satellite communications) bands. Moreover, the proposed antenna is introduced to medical domain, which provides more conveniences and avoids health hazards. Firstly, the antenna design is depicted in Section 2, and detailed analyses for realizing UWB, eliminating the mutual coupling, and adding four frequently-used stopbands are illustrated. Later, the fabrication and measurement results of the proposed antenna are presented in Section 3. Then, the medical application scenario of the proposed design is depicted in Section 4. In the end, Section 5 summarizes this work.

* Corresponding author: Liangliang Zhao (zll18@mail.nwpu.edu.cn).

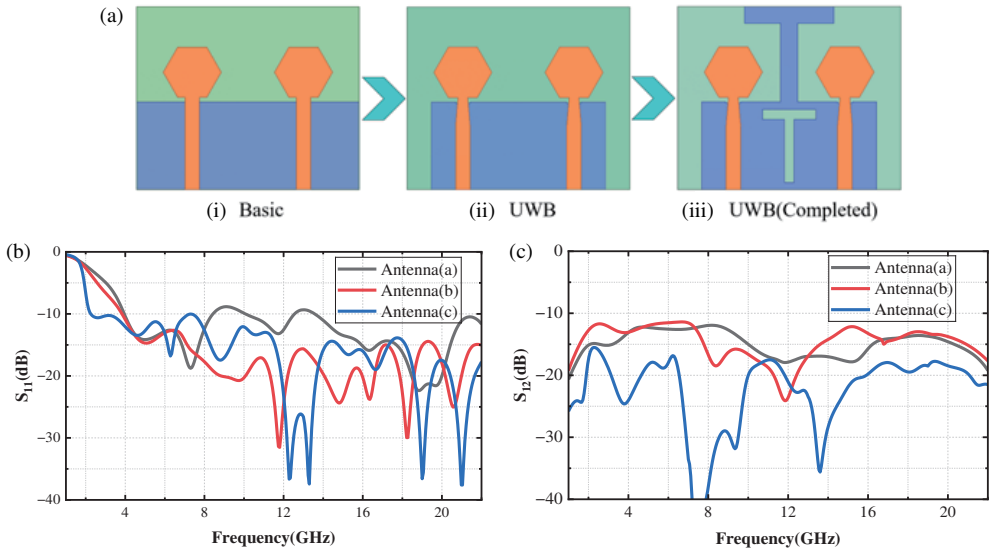

FIGURE 1. (a) The evolution of the reference antenna. (b) The simulated S_{11} varying with the evolution of the antenna. (c) The simulated S_{12} varying with the evolution of the antenna.

2. ANTENNA DESIGN AND PARAMETRIC STUDY

The dimension of the UWB antenna is shown in Fig. 1, and it is fabricated on a $46 \times 37\,\text{mm}^2$ FR4 dielectric substrate with a relative dielectric constant of 4.4 and a thickness of 0.7 mm. A tapered microstrip feedline is employed for exciting the identical hexagon-shaped patch. Then, by adding T-shaped structures and etching T-shaped slots, the mutual coupling is suppressed to attain a high isolation and broaden the operational bandwidth. By etching circle slots and several U-shaped slots, the four frequently-used stopbands are achieved, respectively. It is worth noting that the evolution of the designed dual-port monopole MIMO antenna is illustrated across four steps, i.e., A1 to A4. In the first part, the development of the UWB antenna is depicted. Then, the generation of the four stopbands is described gradually, and the proposed antenna configuration is shown in the last last subsection of this section.

2.1. UWB Monopole Antenna

The following steps elaborate the evolution of the UWB dual-port antenna, as shown in Fig. 1(a). By miniaturizing the ground plane, using a tapered feedline, and etching slots on the ground plane, it is observed that several resonances occur at around 9 GHz, 13 GHz in Fig. 1(b), indicating that the antenna has an ultra-wide bandwidth from 4 GHz to 22 GHz. Unfortunately, the mutual coupling is still deteriorated over the operational bandwidth. It means that the method alone is insufficient in resolving the mutual coupling deterioration problem. Then, employing a T-shaped structure and etching a T-shaped slot on the ground plane, the mutual coupling is improved less than -15 dB over the bandwidth in Fig. 1(c). At the same time, the bandwidth is broadened with a fractional bandwidth covering from 2 to 22 GHz.

2.2. Notched Band Monopole Antenna

(a) First-stopband antenna (Ant. A1)

Figure 2 shows the four design processes of several notch structures, respectively. For clarity, the four notched structures are functioned in Ant. A0 from Fig. 2(b) to Fig. 2(l), respectively. Firstly, the antenna with one stopband is presented in Fig. 2(a)(i). By etching circle slots in the hexagon-shaped patches, a stopband is obtained at around 3.6 GHz, which is called WiMax band. In the meantime, the isolation still retains a low value covering the whole bandwidth.

(b) Second-stopband antenna (Ant. A2)

Moreover, the second stopband is attained at frequency of 5.5 GHz covering from 5.2 GHz to 5.85 GHz by utilizing a U-shaped slot in the tapered feedline in Fig. 2(a)(ii). Although the second stopband relies on the position and length of U-shaped slots, the parameter is optimized to make S_{11} less than -10 dB covering the whole band. In addition, the mutual coupling still retains a great performance within the acceptance range.

(c) Third-stopband antenna (Ant. A3)

Furthermore, Ant. A3 employs two same pairs of U-shaped slots on the outside of the feedline part obtains a stopband at around 7.5 GHz, which is called satellite downlink band. Because of the short distance to feedline part, there are slight influences on the higher frequency band.

(d) Fourth-stopband antenna (Ant. A4)

In addition, the small U-shaped slots etched on the ground plane provide the ITU 8 GHz stopband. It has a bit of an influence on reflection coefficient. As a consequence, the monopole antenna with the notched structure attains a bandwidth ranging from 2 GHz to 22 GHz.

(e) Final design (Ant. A5)

Based on Ant. A0, four antennas, Ant. A1, Ant. A2, Ant. A3, and Ant. A4 are integrated to build the final design. Fig. 2(k) and Fig. 2(l) plot the S-parameters, and the final dimensions of parameters are displayed in Table 1. Therefore, the final

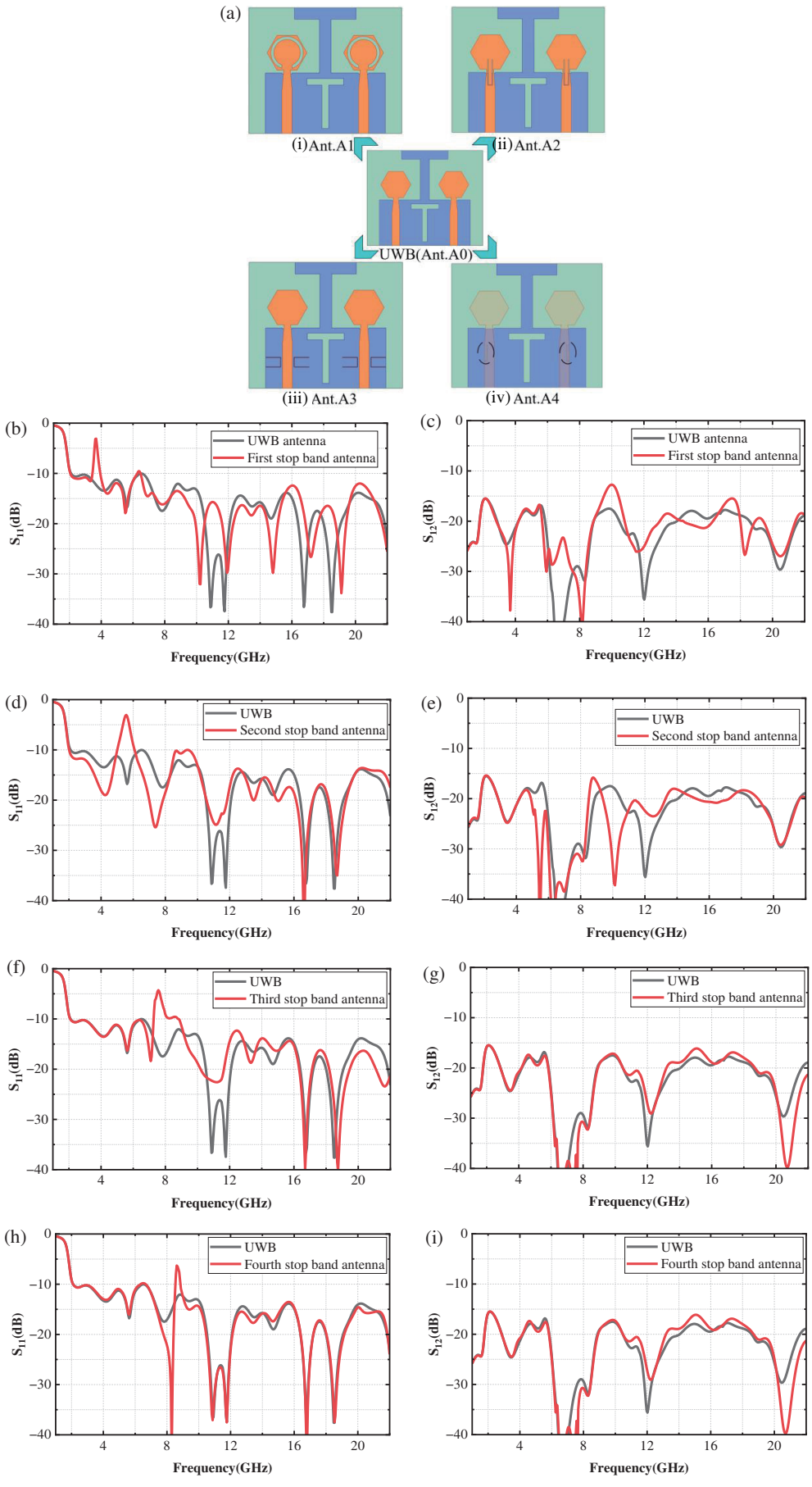
(a)
(i)Ant.A1
(ii)Ant.A2
UWB(Ant.A0)
(iii) Ant.A3
(iv) Ant.A4
(b)
UWB antenna
First stop band antenna
S_{11}(dB)
Frequency(GHz)
(c)
UWB antenna
First stop band antenna
S_{12}(dB)
Frequency(GHz)
(d)
UWB
Second stop band antenna
S_{11}(dB)
Frequency(GHz)
(e)
UWB
Second stop band antenna
S_{12}(dB)
Frequency(GHz)
(f)
UWB
Third stop band antenna
S_{11}(dB)
Frequency(GHz)
(g)
UWB
Third stop band antenna
S_{12}(dB)
Frequency(GHz)
(h)
UWB
Fourth stop band antenna
S_{11}(dB)
Frequency(GHz)
(i)
UWB
Fourth stop band antenna
S_{12}(dB)
Frequency(GHz)

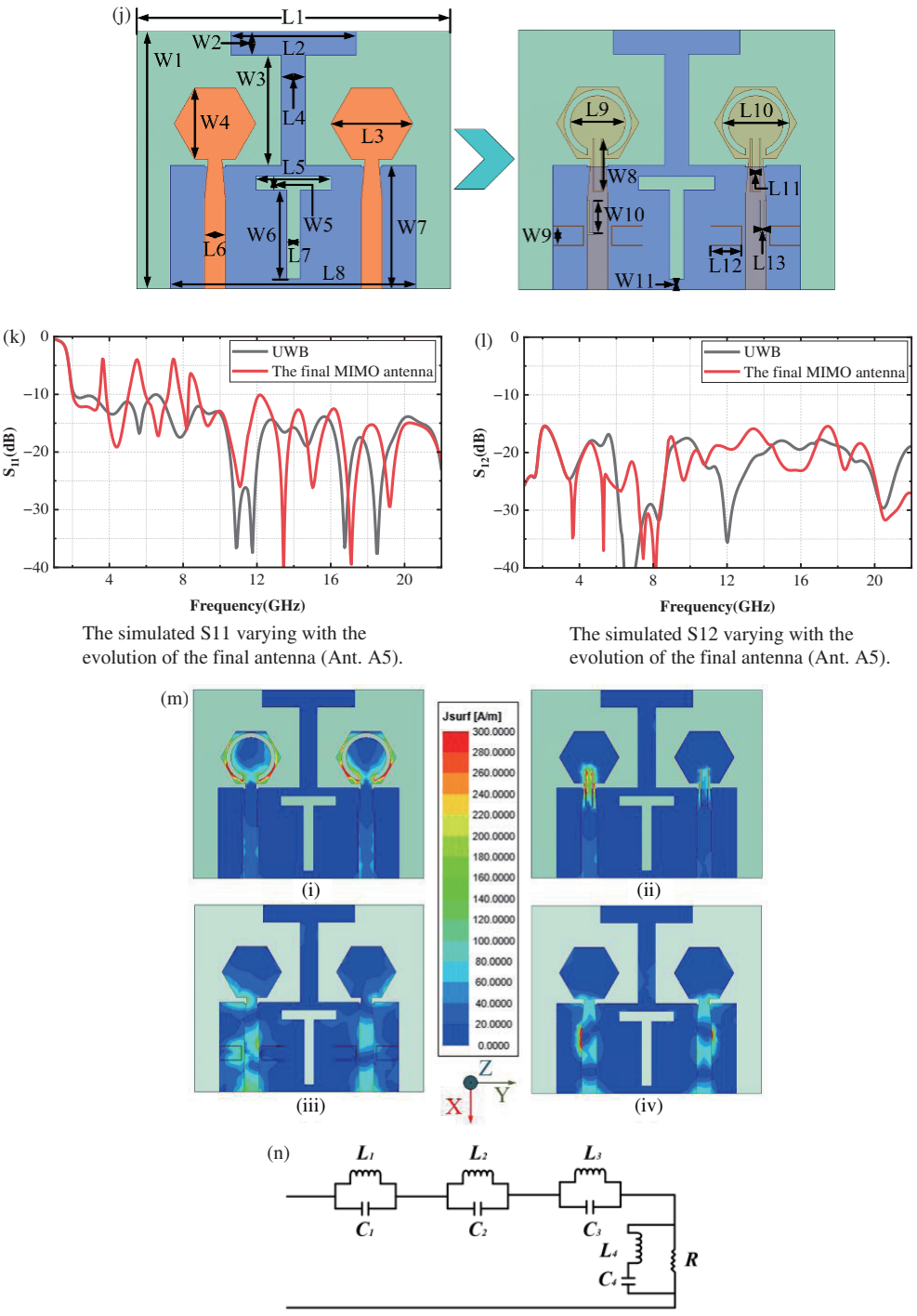

The simulated S11 varying with the evolution of the final antenna (Ant. A5).

The simulated S12 varying with the evolution of the final antenna (Ant. A5).

FIGURE 2. (a) The evolution of the four notched bands antenna. (b) The simulated S_{11} varying with the evolution of the Ant. A1. (c) The simulated S_{12} varying with the evolution of the Ant. A1. (d) The simulated S_{11} varying with the evolution of the Ant. A2. (e) The simulated S_{12} varying with the evolution of the Ant. A2. (f) The simulated S_{11} varying with the evolution of the Ant. A3. (g) The simulated S_{12} varying with the evolution of the Ant. A3. (h) The simulated S_{11} varying with the evolution of the Ant. A4. (i) The simulated S_{12} varying with the evolution of the Ant. A4. (j) Dimension of the proposed antenna (Ant. A5). (k) The simulated S_{11} varying with the evolution of the final antenna (Ant. A5). (l) The simulated S_{12} varying with the evolution of the final antenna (Ant. A5). (m) Magnitude surface current distributions at (i) 3.6, (ii) 5.5, (iii) 7.5, and (iv) 8.4 GHz. (n) The equivalent circuit model of the proposed design.

antenna (Ant. A5) operates in UWB from 2 GHz to 22 GHz integrated with four stopbands at 3.5 GHz (3.47 to 3.83 GHz), 5.5 GHz (5.2–5.85 GHz), 7.5 GHz (7.19–7.84 GHz), and 8.3 GHz (8.15–8.6 GHz). All values are improved owing to the combined impacts of all the structures whereas the modifications are slight. Compared with the UWB-MIMO antenna (Ant. A0), the results are helpful to understand stopbands

TABLE 1. Value of optimized parameters of the final antenna.

Parameter	$L1$	$L2$	$L3$	$L4$	$L5$	$L6$	$L7$	$L8$
Value (mm)	46	18.4	12	3.5	11	3	2	36
Parameter	$L9$	$L10$	$L11$	$L12$	$L13$	$W1$	$W2$	$W3$
Value (mm)	8	9.8	1.5	4.5	0.6	37	3.5	16.15
Parameter	$W4$	$W5$	$W6$	$W7$	$W8$	$W9$	$W10$	$W11$
Value (mm)	10.4	2	13	18.1	7.77	2.7	5	1.5

clearly. The value of isolation is below -20 dB covering the whole band besides low-frequency band, less than -15 dB.

The number of notched bands gradually increases from structures 1 to 4, and the stop frequency band changes to the upper frequency, which describes that the notch performance of the design is gradually distinct.

Ant. A5 with four popular notched bands is the final edition of the proposed UWB MIMO antenna. The dimension of monopole antenna is 46 mm $\times$ 37 mm $\times$ 1.57 mm. HFSS 2021 software is used to design and verify the final design, and the characteristics of the antenna can be depicted obviously. The surface current distributions at four stop frequency points are presented in Fig. 2(m), where (i), (ii), (iii), and (iv) show the current distribution of the proposed antenna at 3.6, 5.5, 7.5, 8.4 GHz, respectively. At 3.6 GHz, the current is mainly contributed on the hexagon-shaped patches. Then, at 5.5 GHz, more currents flow into the U-shaped slots outside the feedline. Meanwhile, at 7.5 GHz, the surface current is mostly concentrated on the U-shaped slot etched in the feedline. Furthermore, at 8.4 GHz, more current is mostly concentrated on the small U-shaped slots etched on the ground plane. The entire notched structure boosts the achievement of four frequently-used stopbands and makes miniaturization possible. To further explain the proposed design clearly, the equivalent circuit model of the proposed design with four different stopbands is presented in Fig. 2(n).

3. SIMULATED AND MEASURED RESULTS

The fabrication model and experimental result are shown in Fig. 3(a) and Fig. 3(b), respectively. Fig. 3(b) gives the simulated results of the final design, which presents the magnitude of the reflection coefficient ($|S_{11}|$) from the four notch bands UWB antenna. With some variances, the measured and simulated S_{11} are mainly close. This is because of several manufacturing errors in the practical environments. The bandwidth of $S_{11} < -10$ dB is from 2 to 22 GHz. In the meantime, the measured isolation of less than -15 dB is obtained throughout the working bandwidth. The stopbands of the final design are 3.47–3.83 GHz, 5.2–5.85 GHz, 7.19–7.84 GHz, and 8.15–8.6 GHz, respectively, which can effectively block the corresponding undesired signals, such as WiMax, WLAN, satellite downlink, and ITU 8 GHz bands. The entire performance illustrates that the proposed antenna obtains superior band-notched performances and great isolation. Furthermore, the fluctuation of S-parameters for the proposed antenna at several frequencies between simulations and measurements is attributed to the flaws of processing and measurement. Fig. 3(c) depicts the radiation pattern of final design at 3 GHz, 4.5 GHz, and 6 GHz. In XOY and YOZ planes, it can be seen that the pattern is quasi-omnidirectional. Furthermore, in XOZ plane, the pattern is bidirectional. Meanwhile, at the main beam direction, the measured cross polarization is below -20 dB. In addition, the measured and simulated results are in great agreement, confirming that the proposed design attains good radiation characteristics.

When the first port is stimulated and the second port terminated, radiation efficiency and realized gain of the simulated and measured antenna are plotted in Fig. 3(d) and Fig. 3(e), respectively. In all four stop frequency bands, the values of realized gain are negative, which indicates that final design obtains superior stop characteristics. In other operational frequency bands, the realized gain surpasses 0, showing that the proposed design attains excellent performances. It is observed that minimum gain and minimum efficiency are achieved at the notch bands. The maximum value of each stopband is larger than -5 dBi, indicating the great notch characteristic of the antenna. Meanwhile, the peak gain of the proposed antenna can exceed 4 dBi. Besides, the radiation efficiency value illustrates that the efficiency of the bandwidth is continuously above 75% and keeps a high value, excluding the stopbands. The final design attains a perfect omnidirectional characteristic, and there are slight discrepancies at high band. Although there are several differences, it is visible that the measured and simulated results are relatively close. Meanwhile, the final design has lower ECC value as shown in Fig. 3(f), which is less than 0.005.

$$ECC = \frac{\left|S_{11}^{*}S_{12} + S_{21}^{*}S_{22}\right|^{2}}{\left(1-\left|S_{11}\right|^{2}-\left|S_{21}\right|^{2}\right)\left(1-\left|S_{22}\right|^{2}-\left|S_{12}\right|^{2}\right)} \quad (1)$$

The characteristics of the final design are listed with other previous studies. As seen in Table 2, the proposed antenna obtains four frequently-used stopbands than those presented in previous literature. Meanwhile, it has a wider operational bandwidth covering from 2 to 22 GHz. Moreover, it has a more miniaturized size of $0.3\lambda_{\text{low}} \times 0.24\lambda_{\text{low}} \times 0.01\lambda_{\text{low}}$ than other studies. All performances of the proposed antenna show a great competitiveness when it comes to size, stopband number, bandwidth, prompting it as a strong candidate in MIMO UWB antenna application.

4. MEDICAL APPLICATION OF THE PROPOSED ANTENNA

In medical domain, if the name badge is always taken off and picked up, the risk of bacterial pollution will gradually increase.

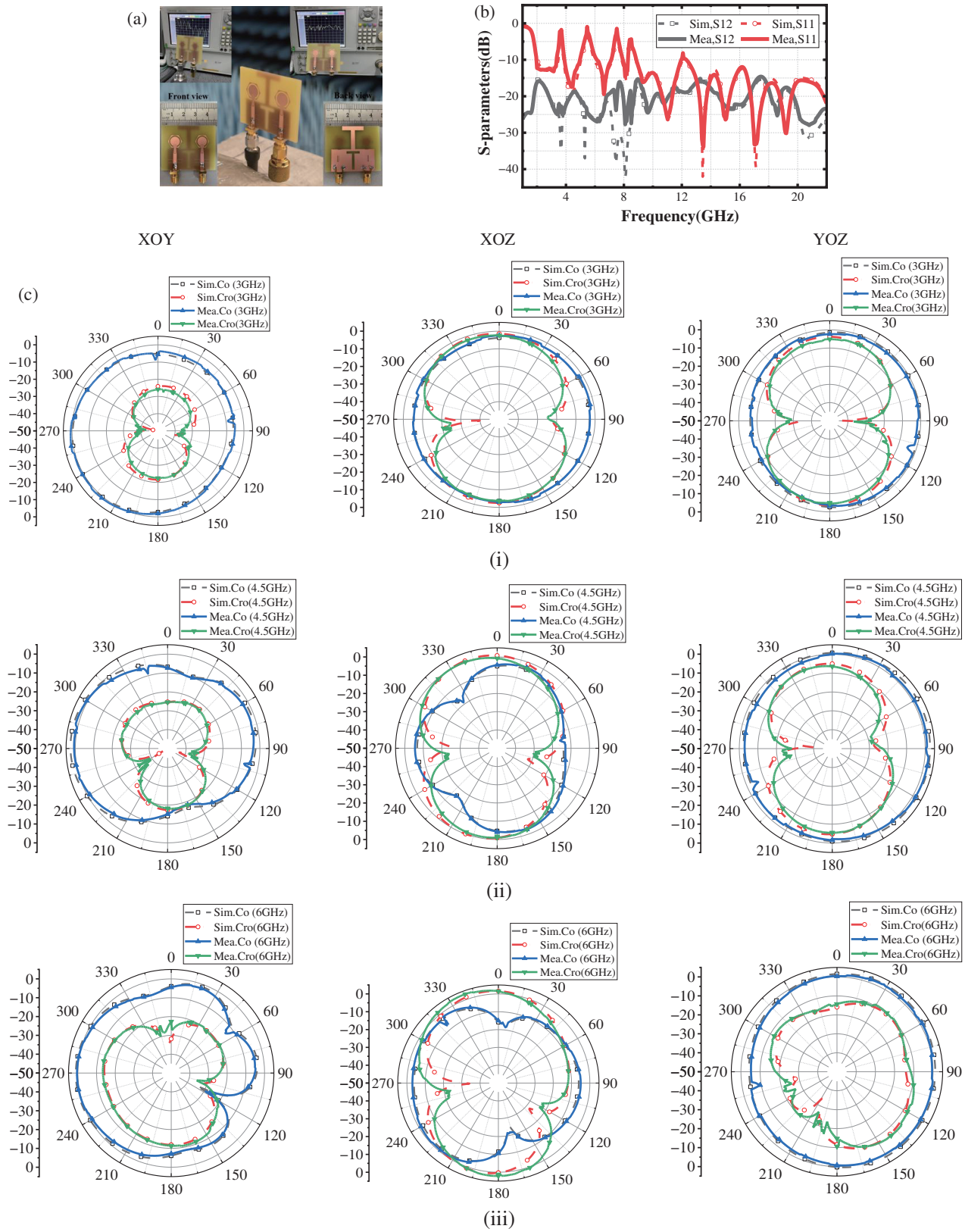

(i) 3GHz. (ii) 4.5GHz. (iii) 6GHz.

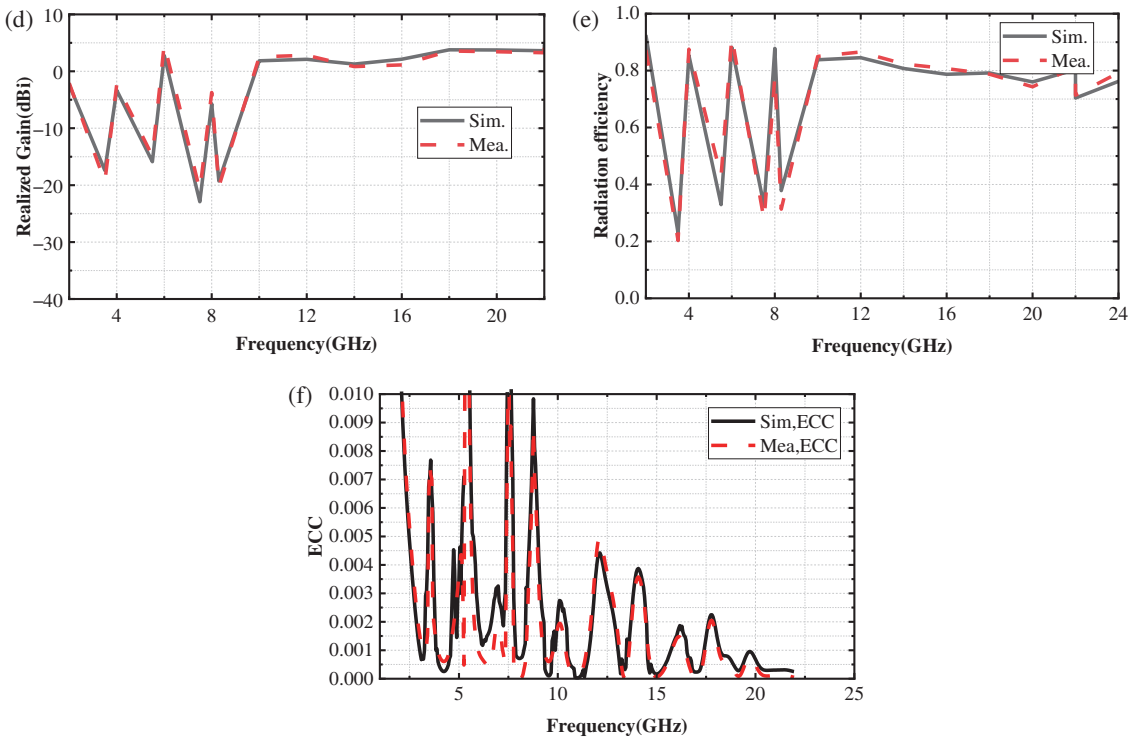

FIGURE 3. (a) Fabricated antenna and its measurement view. (b) The simulated and measured S-parameters of the proposed antenna. (c) Simulated and measured radiation patterns of XOY, XOZ, YOZ planes. (d) Simulated and measured Realized Gain. (e) Simulated and measured Radiation efficiency. (f) Simulated and measured ECC varying with frequency.

TABLE 2. Performance comparison of different antennas.

Ref.	Dimension	Bandwidth	Num. notch bands	ECC	Gain (dBi)	Efficiency
[27]	$0.214\lambda_{low} \times 0.256\lambda_{low} \times 0.004\lambda_{low}$ (30 mm × 25 mm × 0.508 mm)	2.56–12.7	5	NG	4.76	> 75%
[28]	$0.383\lambda_{low} \times 0.383\lambda_{low} \times 0.009\lambda_{low}$ (35.9 mm × 35.9 mm × 0.8 mm)	3.2–10.8	3	< 0.49	4.7	> 80%
[29]	(35 mm × 46 mm × 1.575 mm)	2.1–11.4	2	< 0.04	NG	> 75%
[30]	$0.25\lambda_{low} \times 0.25\lambda_{low} \times 0.006\lambda_{low}$ (30 mm × 30 mm × 0.7 mm)	2.5–10.8	2	< 0.004	4.9	> 80%
[31]	$0.245\lambda_{low} \times 0.192\lambda_{low} \times 0.008\lambda_{low}$ (46 mm ∗ 36 mm ∗ 1.59 mm)	1.6–16	2	< 0.1	NG	NG
This work	$0.3\lambda_{low} \times 0.24\lambda_{low} \times 0.01\lambda_{low}$ (46 mm × 37 mm × 1.57 mm)	2–22 GHz	4	< 0.005	4.4	> 75%

To avoid these issues, the proposed antenna can be integrated with the name badge, which offers more conveniences and keeps the original appearances.

In general, the SAR value is a significant standard that determines whether the antenna can be used due to the closed distance to body. Therefore, the SAR level simulated models are presented in Fig. 4(a). Generally, skin, fat, and muscle constitute the human body. In the meantime, the thicknesses of the three tissues are 1, 5, and 20 mm, respectively. In addition, a 10 mm air layer between antenna and body is suitable, which is a common gap in reality. Furthermore, the SAR value must be maintained below 1.6 W/kg per 1 g tissue from IEEE C95.1-1999 standard. Furthermore, the 3D SAR distributions of the proposed monopole antenna at 2, 4, and 6 GHz are shown in Fig. 4(b), respectively. Besides, Table 3 concludes the maximum possible power of the proposed antenna within the IEEE standard. In total, the superior performance of the proposed antenna can integrate well with name badge, and wearing it on the chest is reliable enough for human health.

TABLE 3. Maximum SAR and maximum input power.

Frequency (GHz)	1 g Tissue [W/kg]/Input power [W]
2	1.52/0.08
4	1.54/0.11
6	1.49/0.25

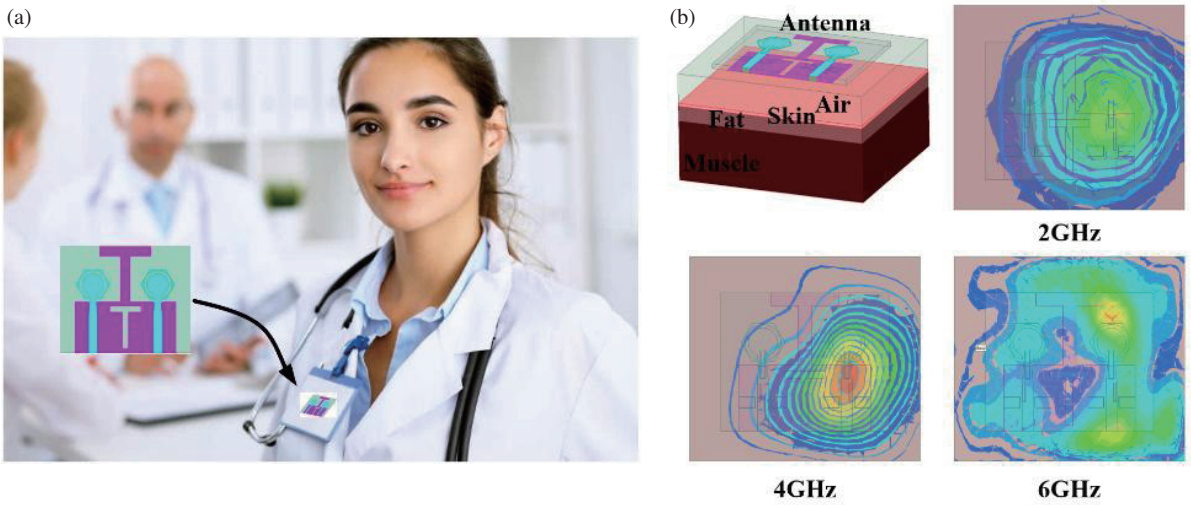

FIGURE 4. (a) Application of the proposed antenna. (b) Illustration of the proposed antenna over the human tissue in HFSS and SAR distributions at 2, 4, 6 GHz.

5. CONCLUSION

A miniaturized dual-port UWB MIMO hexagon-shaped monopole antenna integrated with four popular frequently-used stopbands is designed. First, the proposed design achieves a UWB operational frequency ranging from 2 to 22 GHz. Next, utilizing stop structures etched on the radiation patch and feedline, loading U-shaped slots, and etching slots in the ground plane, a four stopbands antenna is realized. Meanwhile, step-by-step configuration and accomplishment of results are presented in detail. Moreover, the final design attains an overall dimension of $0.3\lambda_{low} \times 0.24\lambda_{low} \times 0.01\lambda_{low}$ ($46\,\text{mm} \times 37\,\text{mm} \times 1.57\,\text{mm}$), showing the miniaturized design. The experimental results show that the final design can cover the whole UWB spectrum except stopbands from 3.47 to 3.83 GHz (WiMax), 5.2 to 5.85 GHz (WLAN), 7.19 to 7.84 GHz (satellite downlink), 8.15 to 8.6 GHz (ITU 8 GHz). Then, the value of ECC is less than 0.005, whereas experimentally isolation is below -20 dB in the almost the whole operational band. Totally, all results indicate that the huge potential of the proposed design can be extensively used in UWB-MIMO wireless communication system for portable fields, such as name badge of the doctor and relevant medial field.

REFERENCES

[1] Chahat, N., M. Zhadobov, R. Sauleau, and K. Ito, "A compact UWB antenna for on-body applications," *IEEE Transactions on Antennas and Propagation*, Vol. 59, No. 4, 1123–1131, 2011.

[2] Tang, M.-C., T. Shi, and R. W. Ziolkowski, "Planar ultrawideband antennas with improved realized gain performance," *IEEE Transactions on Antennas and Propagation*, Vol. 64, No. 1, 61–69, 2016.

[3] Gómez-Villanueva, R. and H. Jardón-Aguilar, "Compact UWB uniplanar four-port MIMO antenna array with rejecting band," *IEEE Antennas and Wireless Propagation Letters*, Vol. 18, No. 12, 2543–2547, 2019.

[4] Khandelwal, M. K., B. K. Kanaujia, and S. Kumar, "Defected ground structure: Fundamentals, analysis, and applications in modern wireless trends," *International Journal of Antennas and Propagation*, Vol. 2017, No. 1, 2018527, 2017.

[5] Liu, L., S. W. Cheung, and T. I. Yuk, "Compact MIMO antenna for portable UWB applications with band-notched characteristic," *IEEE Transactions on Antennas and Propagation*, Vol. 63, No. 5, 1917–1924, 2015.

[6] Chandel, R., A. K. Gautam, and K. Rambabu, "Tapered fed compact UWB MIMO-diversity antenna with dual band-notched characteristics," *IEEE Transactions on Antennas and Propagation*, Vol. 66, No. 4, 1677–1684, 2018.

[7] Zhu, J., S. Li, B. Feng, L. Deng, and S. Yin, "Compact dual-polarized UWB quasi-self-complementary MIMO/diversity antenna with band-rejection capability," *IEEE Antennas and Wireless Propagation Letters*, Vol. 15, 905–908, 2015.

[8] Tang, Z., J. Zhan, X. Wu, Z. Xi, L. Chen, and S. Hu, "Design of a compact UWB-MIMO antenna with high isolation and dual band-notched characteristics," *Journal of Electromagnetic Waves and Applications*, Vol. 34, No. 4, 500–513, 2020.

[9] Hassan, M. M., M. Rasool, M. U. Asghar, Z. Zahid, A. A. Khan, I. Rashid, A. Rauf, and F. A. Bhatti, "A novel UWB MIMO antenna array with band notch characteristics using parasitic decoupler," *Journal of Electromagnetic Waves and Applications*, Vol. 34, No. 9, 1225–1238, 2020.

[10] Liu, H., G. Kang, and S. Jiang, "Compact dual band-notched UWB multiple-input multiple-output antenna for portable applications," *Microwave and Optical Technology Letters*, Vol. 62, No. 3, 1215–1221, 2020.

[11] Deng, J.-Y., L.-X. Guo, and X.-L. Liu, "An ultrawideband MIMO antenna with a high isolation," *IEEE Antennas and Wireless Propagation Letters*, Vol. 15, 182–185, 2015.

[12] Kang, L., H. Li, X. Wang, and X. Shi, "Compact offset microstrip-fed MIMO antenna for band-notched UWB applications," *IEEE Antennas and Wireless Propagation Letters*, Vol. 14, 1754–1757, 2015.

[13] Toktas, A., "G-shaped band-notched ultra-wideband MIMO antenna system for mobile terminals," *IET Microwaves, Antennas & Propagation*, Vol. 11, No. 5, 718–725, 2017.

[14] Kumar, A., A. Q. Ansari, B. K. Kanaujia, J. Kishor, and S. Kumar, "An ultra-compact two-port UWB-MIMO antenna with dual band-notched characteristics," *AEU — International Journal of Electronics and Communications*, Vol. 114, 152997, 2020.

[15] Bhattacharya, A., B. Roy, S. K. Chowdhury, and A. K. Bhattacharjee, "An isolation enhanced, printed, low-profile UWB-MIMO antenna with unique dual band-notching features for WLAN and WiMAX," *IETE Journal of Research*, Vol. 68, No. 1, 496–503, 2022.

[16] Agarwal, M., J. K. Dhanoa, and M. K. Khandelwal, "Ultrawide band two-port MIMO diversity antenna with triple notch bands, stable gain and suppressed mutual coupling," *AEU — International Journal of Electronics and Communications*, Vol. 120, 153225, 2020.

[17] Gao, P., S. He, X. Wei, Z. Xu, N. Wang, and Y. Zheng, "Compact printed UWB diversity slot antenna with 5.5-GHz band-notched characteristics," *IEEE Antennas and Wireless Propagation Letters*, Vol. 13, 376–379, 2014.

[18] Liu, L., S. W. Cheung, and T. I. Yuk, "Compact MIMO antenna for portable devices in UWB applications," *IEEE Transactions on Antennas and Propagation*, Vol. 61, No. 8, 4257–4264, 2013.

[19] Zhao, L., C. Liu, C. Li, D. Song, Y. Wang, Y. Liang, H. Zhao, and C. Hu, "A novel helical antenna for high-power design in X-band," *AEU — International Journal of Electronics and Communications*, Vol. 168, 154725, 2023.

[20] Awan, W. A., A. Zaidi, N. Hussain, A. Iqbal, and A. Baghdad, "Stub loaded, low profile UWB antenna with independently controllable notch-bands," *Microwave and Optical Technology Letters*, Vol. 61, No. 11, 2447–2454, 2019.

[21] Iqbal, A., A. Smida, N. K. Mallat, M. T. Islam, and S. Kim, "A compact UWB antenna with independently controllable notch bands," *Sensors*, Vol. 19, No. 6, 1411, 2019.

[22] Kumar, G., D. Singh, and R. Kumar, "A planar CPW fed UWB antenna with dual rectangular notch band characteristics incorporating U-slot, SRRs, and EBGs," *International Journal of RF and Microwave Computer-Aided Engineering*, Vol. 31, No. 7, e22676, 2021.

[23] Ahasan, S. k. R., K. Islam, M. M. Khan, M. Masud, G. S. Gaba, and H. A. Alhumyani, "Novel compact UWB band notch antenna design for body-centric communications," *Computer Systems Science & Engineering*, Vol. 40, No. 2, 673–689, 2022.

[24] Kumar, O. P., P. Kumar, and T. Ali, "A compact dual-band notched UWB antenna for wireless applications," *Micromachines*, Vol. 13, No. 1, 12, 2022.

[25] Cui, L., H. Liu, C. Hao, and X. Sun, "A novel UWB antenna with triple band-notches for WiMAX and WLAN," *Progress In Electromagnetics Research Letters*, Vol. 82, 101–106, 2019.

[26] Devana, V. N. K. R. and A. M. Rao, "A novel fan shaped UWB antenna with band notch for WLAN using a simple parasitic slit," *International Journal of Electronics Letters*, Vol. 7, No. 3, 352–366, 2019.

[27] Zhao, Z., C. Zhang, Z. Lu, H. Chu, S. Chen, M. Liu, and G. Li, "A miniaturized wearable antenna with five band-notched characteristics for medical applications," *IEEE Antennas and Wireless Propagation Letters*, Vol. 22, No. 6, 1246–1250, 2023.

[28] Jayant, S. and G. Srivastava, "Close-packed Quad-element triple-band-notched UWB MIMO antenna with upgrading capability," *IEEE Transactions on Antennas and Propagation*, Vol. 71, No. 1, 353–360, 2023.

[29] Agarwal, M., J. K. Dhanoa, and M. K. Khandelwal, "Two-port hexagon shaped MIMO microstrip antenna for UWB applications integrated with double stop bands for WiMax and WLAN," *AEU — International Journal of Electronics and Communications*, Vol. 138, 153885, 2021.

[30] Yuan, H., F.-S. Zhang, J.-J. Zhang, Y.-X. Feng, and Y.-F. Liu, "A compact ultra-wideband multiple-input-multiple-output antenna with dual band-notched performance using slot-line transmission," *International Journal of RF and Microwave Computer-Aided Engineering*, Vol. 32, No. 5, e23098, 2022.

[31] Zhao, L., Y. Wang, C. Liu, D. Song, C. Hu, C. Li, H. Zhao, and Z. Wang, "Compact circular-shaped MIMO antenna covers UWB bandwidth with four frequently-used band-notched characteristics for multi-scenario applications," *IEEE Access*, Vol. 12, 32 762–32 771, 2024.

[32] Kholapure, A. and R. G. Karandikar, "Printed MIMO antenna with reconfigurable single and dual band notched characteristics for cognitive radio," in *2017 IEEE International Conference on Antenna Innovations & Modern Technologies for Ground, Aircraft and Satellite Applications (iAIM)*, 1–5, 2017.

[33] Zhao, L., H. Zhu, C. Ding, G. Liu, H. Zhao, J. Mou, and Y. J. Guo, "An ultrawideband dual-polarized tightly coupled dipole array (TCDA) with wide scanning range," *IEEE Antennas and Wireless Propagation Letters*, Vol. 23, No. 7, 1961–1965, 2024.

[34] Zhu, H., G. Liu, L. Zhao, J. Xu, Y. Di, and H. Zhao, "Ultrawideband, dual-linearly polarized tightly coupled dipole array with composite wide-angle scanning superstrate," in *2023 IEEE International Symposium On Antennas And Propagation (ISAP)*, 1–2, Kuala Lumpur, Malaysia, 2023.

[35] Zhao, L.-L., C. Hu, C. Fang, C. Fan, J. Li, and A. Li, "Grid restoration algorithm to improve PO calculation accuracy in GRECO," in *2020 Cross Strait Radio Science & Wireless Technology Conference (CSRSWTC)*, 1–3, Fuzhou, China, 2020.

[36] Li, J., L. Zhao, X. Liu, and Y. Li, "FSV-based evaluation of electromagnetic scattering characteristics of deformed target," in *2019 International Applied Computational Electromagnetics Society Symposium — China (ACES)*, Vol. 1, 1–2, Nanjing, China, 2019.

[37] Zhao, L., Y. Wang, D. Song, C. Liu, C. Li, H. Zhao, and C. Hu, "Compact Vivaldi antenna application in high-power design at X-band," in *2024 18th European Conference on Antennas and Propagation (EuCAP)*, 1–3, Glasgow, United Kingdom, 2024.

[38] Yang, M., H. Peng, K. Zheng, and G. Wei, "Spatial radiation field distribution of underwater VLF two-element antenna array," *IEEE Transactions on Antennas and Propagation*, Vol. 71, No. 1, 1164–1169, 2023.

[39] Saurabh, A. K., R. Dubey, and M. K. Meshram, "Wideband eight-element MIMO antenna with band-dispensation characteristics," *AEU — International Journal of Electronics and Communications*, Vol. 155, 154344, 2022.

[40] Zhao, L., H. Zhu, H. Zhao, G. Liu, K. Wang, J. Mou, W. Zhang, and J. Li, "Design of wideband dual-polarized ME dipole antenna with parasitic elements and improved feed structure," *IEEE Antennas and Wireless Propagation Letters*, Vol. 22, No. 1, 174–178, 2023.

[41] Yang, M., Q. Wu, K. Zheng, S. Zhang, and G. Wei, "Radiation field distribution above sea surface of underwater microstrip antenna array," *IEEE Antennas and Wireless Propagation Letters*, Vol. 23, No. 2, 858–862, 2024.